Structural, microstructural, and thermal characterizations of a chalcopyrite concentrate from the Singhbhum shear zone, India

Ritayan Chatterjee[1,2]*, Shamik Chaudhuri*[1]*, Saikat Kumar Kuila*[1]*, and Dinabandhu Ghosh*[1]

1) Department of Metallurgical and Materials Engineering, Jadavpur University, Kolkata 700032, India

2) Division of Materials Engineering, Lund University, Box 118, SE-22100 Lund, Sweden

Abstract: The structural and morphological characterizations of a chalcopyrite concentrate, collected from the Indian Copper Complex, Ghatshila, India, were carried out by X-ray diffraction, scanning electron microscopy, and energy-dispersive X-ray spectroscopy. The concentrate powder was composed mainly of free chalcopyrite and low quartz in about 3:1 weight ratio. The particle size was about 100 μm. Spectroscopic studies (FTIR, Raman, UV-visible) of the concentrate supported the XRD findings, and also revealed a marginal oxidation of the sulfide phase. The energy band gap of the sulfide was found to be 3.4 eV. Differential thermal analysis and thermogravimetry of the concentrate showed a decomposition of chalcopyrite at 658 K with an activation energy of 208 kJ·mol^{-1}, and two successive structural changes of silica at 848 K and 1145 K.

Keywords: chalcopyrite; structural properties; microstructure; thermal characteristics

1. Introduction

The principal copper ores in nature are sulfides among which chalcopyrite ($CuFeS_2$) is the major source of copper [1]. Chalcopyrite contains many minerals including copper, iron, zinc, and sulfur. Chalcopyrite is the most stable mineral among the copper sulfides due to its structural configuration (face-centered tetragonal lattice). Chalcopyrite ores are usually processed by means of hydrometallurgical or pyrometallurgical processes, but due to environmental aspects there has been a worldwide upsurge of interest in the hydrometallurgical processes of this ore [2]. Alternatively, the hydrogen reduction technique has been incorporated as an environment-friendly pyrometallurgical route [3]. The different concentrates obtained through differential flotation, which are used in pyrometallurgy, are usually of poor quality with low metal recovery [4]. A good idea about the composition and physical properties of the ore or the concentrate is necessary to choose the proper extraction technique, especially in the pyrometallurgical processing.

The chalcopyrite concentrate characterized in the present study was collected from Ghatshila, in the Singhbhum shear zone, India. The Singhbhum copper belt comprises Proterozoic volcano-sedimentary rocks that created a shear zone known as the Singhbhum shear zone. Prominent deposits of the belt are the Chapri, Rakha, Surda, Kendadih, Pathargora, and Dhobani. The first copper mine in this region was established in 1930. The chalcopyrite concentrate is brownish-yellow in appearance with good luster, and granular in nature. The concentrate contains more than 16wt.% of copper.

The objective of the present work was to characterize the chalcopyrite concentrate by X-ray diffraction, microscopy, spectroscopy, and thermal analysis in order to support the selection of beneficiation process in recovering copper values. For this purpose, the crystallographic phases were identified by the diffraction study and a two-phase Rietveld refinement of the diffraction data. The spectroscopic studies were carried out in the infrared and ultraviolet-visible regions, and by Raman spectroscopy. The morphology of the mineral was studied by scanning electron microscopy (SEM)

🖄 Springer

with simultaneous energy-dispersive X-ray spectroscopy. The thermal property of the concentrate was studied by thermogravimetric and differential thermal analysis techniques.

2. Experimental

2.1. Materials

The chalcopyrite concentrate used in the present study was collected from the Indian Copper Corporation Ltd. (ICC), Ghatsila, India.

2.2. Methods

Powder X-ray diffraction (XRD) of the chalcopyrite concentrate was recorded by a vertical STOE Stadi MP diffractometer using transmission geometry and Cu K$_\alpha$ (λ = 0.154184 nm) radiation. The generator settings were 40 kV and 40 mA. The diffraction patterns were recorded at room temperature (293 K), step size of 0.1°, stoppage time of 10 s per step, and range of 2θ = 18–92°. Cylindrical compacts of the concentrate powder were formed using a stainless steel die, and scanning electron microscopic (SEM) images of the planar surfaces were captured using a Philips XL–30 ESEM microscope. An elemental mapping for the major elements (Cu, Fe, S, Si, and O) was obtained by the attached EDAX energy-dispersive X-ray spectroscope (EDX) system. Particle size distribution was obtained using the standard sieve analysis. Fourier-transform infrared (FTIR) spectra of the chalcopyrite concentrate were obtained adopting the KBr pellet technique, using a FTIR spectroscope (IR prestige 21, 200V CE, Shimadzu, Tokyo, Japan). Approximately 2 mg of the concentrate powder was thoroughly mixed with 200 mg of spectroscopic-grade KBr and pressed into pellets. Raman spectra of the concentrate were recorded in the Stokes region with the help of a micro-Raman Renishaw spectrometer (UK) at the laser excitation energy of 1.58 eV (785 nm diode laser) at room temperature. Ultraviolet (UV)-visible (vis) absorption spectra of the concentrate were recorded on a Shimadzu UV–1601PC spectrophotometer. Experiments were carried out in 1 cm × 1 cm quartz cuvette containing 2 mL of phosphate buffer. Thermogravimetric (TG) and differential thermal (DT) analyses of the concentrate were carried out at the heating rate of 10 K·min^{-1} in separate DT–TG set-up (Make: Bysakh Co., Brand: Okay). Approximately 300 mg of the concentrate powder in an alumina crucible was used as a sample for both analyses. The same mass of α-alumina powder in a similar crucible was taken as the reference in the DTA. The data were recorded at 20 s interval throughout the heating process.

3. Results and discussion

3.1. Powder XRD analysis

The two-phase Rietveld refinement of the powder XRD pattern of the concentrate is shown in Fig. 1, where the red points represent the experimental values, and the black solid line depicts the calculated values. Vertical bars show the positions of the calculated Bragg reflections, and the blue solid line at the bottom is the difference between the experimental and the calculated values. In the experimental XRD pattern, the majority of the main peaks belong to chalcopyrite, which is the main copper mineral present in the ore. Most of the remaining peaks belong to low quartz, which is the principal impurity phase. The powder XRD profile was fitted for these two phases using the LeBail algorithm [5] implemented in the Jana2006 program [6]. The refined values of the cell parameters, and the phase group with the R factors (R factors predict the quality of Rietveld fit to a powder diffraction pattern), are shown in Table 1. The reliability index parameters and the goodness of fit (GOF) for the refinement are R_p = 3.04, R_{wp} = 5.60, and GOF = 3.39 (R_p and R_{wp} are profile R factor and weighted profile R factor, respectively). The GOF value is not very satisfactory because of the unindexed peaks at 2θ = 24.8°, 28.7°, and 56.2°. These unindexed peaks are from the silicate class clinoferrosilite (FeSiO$_3$), PCPDF # 75–1214, Pearson's Crystal Data Entry number 1616032 with space group $C12/c1$ and cell parameters, a = 0.9928 nm, b = 0.9179 nm, c = 0.5338 nm, α = 90°, β = 110.20°, and γ = 90°. The relative amount of clinoferrosilite is low in the concentrate, and hence, does not significantly affect the refinement results.
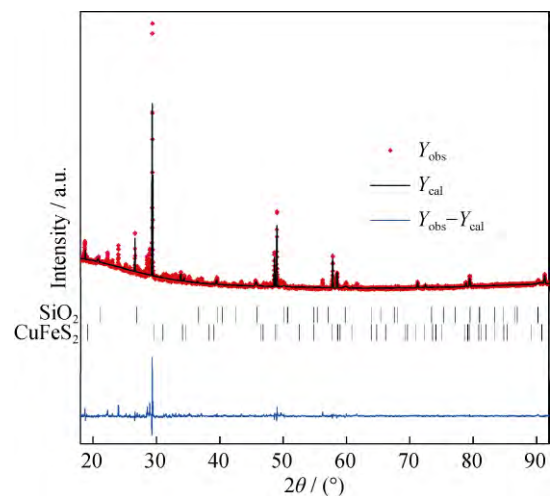
Fig. 1. Two phases Rietveld refinement pattern based on powder XRD at room temperature for chalcopyrite concentrate (Y_{obs} is the experimental value and Y_{cal} is the calculated value).

Table 1. Rietveld refinement of two phases based on powder XRD pattern

Phase	Cell parameters	Phase group	R factors
Chalcopyrite (CuFeS$_2$)	$a = 0.5290181$ nm, $b = 0.5290181$ nm, $c = 1.042317$ nm; $\alpha = 90°, \beta = 90°, \gamma = 90°$	$I\bar{4}2d$	$R(\text{obs}) = 6.68$ $wR(\text{obs}) = 6.11$ $R(\text{all}) = 10.01$ $wR(\text{all}) = 6.88$
Quartz (SiO$_2$)	$a = 0.4920487$ nm, $b = 0.4920487$ nm, $c = 0.5391766$ nm; $\alpha = 90°, \beta = 90°, \gamma = 120°$	$P3121$	$R(\text{obs}) = 6.18$ $wR(\text{obs}) = 5.54$ $R(\text{all}) = 11.09$ $wR(\text{all}) = 5.96$

Note: R and wR indicate reliability index parameters; "obs" indicates observed reflections; "all" indicates all reflections, both strong and weak.

The phase-volume ratio (v_i) of the refinement phases (CuFeS$_2$ to SiO$_2$) was calculated as 1:0.524117. The weight ratio of CuFeS$_2$ to SiO$_2$, calculated from the volume ratio, was 0.753:0.246, using the relation of the relative phase amount (m_i) to v_i:

$$m_i = \frac{v_i \rho_i}{\sum_i v_i \rho_i},$$

where ρ_i is the density of the ith phase.

3.2. SEM, EDX, and particle size

The SEM images taken in secondary electron (SE), and in backscattered electron (BSE) mode of the plane surface of the compact formed from concentrate powder, are shown in Figs. 2(a) and 2(b) respectively. The EDX spectra, taken from the whole area of the SEM images, are shown in Fig. 2(c). The elements present in the concentrate with their weight percentages on the basis of EDX are given in Table 2. The elemental mapping for the major elements (Cu, Fe, S, Si, and O) taken over the surface area captured in SEM images is shown in Figs. 2(d), 2(e), 2(f), 2(g) and 2(h), respectively. In Fig. 2(a) four points are chosen in which point 1 and 2 show chalcopyrite particles, and points 3 and 4 show quartz particles. In the subsequent images, the locations of these points are carried forward. A finite concentration of Cu, Fe, and S, and almost zero concentration of Si at points 1 and 2, help to locate the grains at these points as chalcopyrite. On the other hand, the grains at points 3 and 4 have no Cu, Fe, and S, but have large concentration of Si instead, suggesting that these grains are made of quartz. The concentration of O is high in the high-Si sites, and very low at the sites with high concentration of Cu, Fe, or S. This confirms that the main oxide impurity in the concentrate is quartz. The diameters of chalcopyrite and quartz grains are measured from the SE images. The chalcopyrite grain diameters at points 1 and 2 are 78 and 95 µm, whereas the quartz grain diameters at points 3 and 4 are 102 and 88 µm. These results are in good agreement with the sieve analysis given in Fig. 3. The majority of chalcopyrite particle is below 80 µm, and that of the quartz is below 120 µm.

According to the analysis given in Table 2, 1 g of the concentrate contains 0.0726 g Si = 0.1553 g SiO$_2$ = 2.593 × 10^{-3} mole of SiO$_2$ and 0.1828 g S = 5.701 × 10^{-3} mole of S = 2.85 × 10^{-3} mole of CuFeS$_2$ (considering S is present as CuFeS$_2$ only) = 0.5227 g CuFeS$_2$. The weight ratio of chalcopyrite-to-quartz thus obtained is 0.771:0.229, which is in good agreement with the result obtained from the Rietveld refinement. According to the Rietveld refinement, the preceding ratio is slightly smaller, which can be explained by the partial oxidation of the sulfide.

3.3. Fourier-transform infrared spectroscopic analysis

The FTIR spectrum of the chalcopyrite concentrate is shown in Fig. 4, which was taken in the wavenumber range of 400–2000 cm^{-1} at the room temperature. The principal vibrational modes were assigned and are presented in Table 3. The IR spectrum of sulfides is characterized by the broadened peaks due to the specific features of the crystalline structure, and the nature of Me–S bonds [7]. Chalcopyrite, a ternary compound having the diamond structure with every atom bonded to the four nearest neighbors in a tetrahedron, can be obtained by doubling the zincblende (ZnS) structure. Each atom has four neighbors arranged at the corners of a regular tetrahedron bonded by sp^3 bonds. Each metal atom has four sulfur atoms as the first neighbors, whereas each sulfur atom has two copper and two iron atoms. The spectrum exhibits absorption bands at 1105, 1142, and 1204 cm^{-1}, which indicates the presence of chalcopyrite [8–9] as the principal phase in the concentrate sample. In addition to these bands, the oxidized chalcopyrite sample displays a band at 1010 cm^{-1}, which can be assigned to the S–O stretching vibrations in the sulfide structure [10], while the band at 630 cm^{-1} represents the S–O bend vibrations.

The major impurity phases in the chalcopyrite concentrate are silica and silicates. The symmetric Si–O–Si stretching vibration of the coordinated silica groups appears at 798 cm^{-1} [11], and in addition, there are small absorptions at 781 cm^{-1} and 886 cm^{-1} [12]. The characteristic asymmetric Si–O–Si stretch in the range of 1040–1090 cm^{-1} [13] is masked behind the dominating chalcopyrite absorption. The bending modes of Si–O–Si at 625 cm^{-1}, and the weak ab-

sorption band of Si–O–Si at 580 cm^{-1}, are caused by the presence of $(SiO_4)^{-4}$ groups [11]. The bands observed in the range of 411–515 cm^{-1} can be attributed to the Si–O–Si absorption [14].
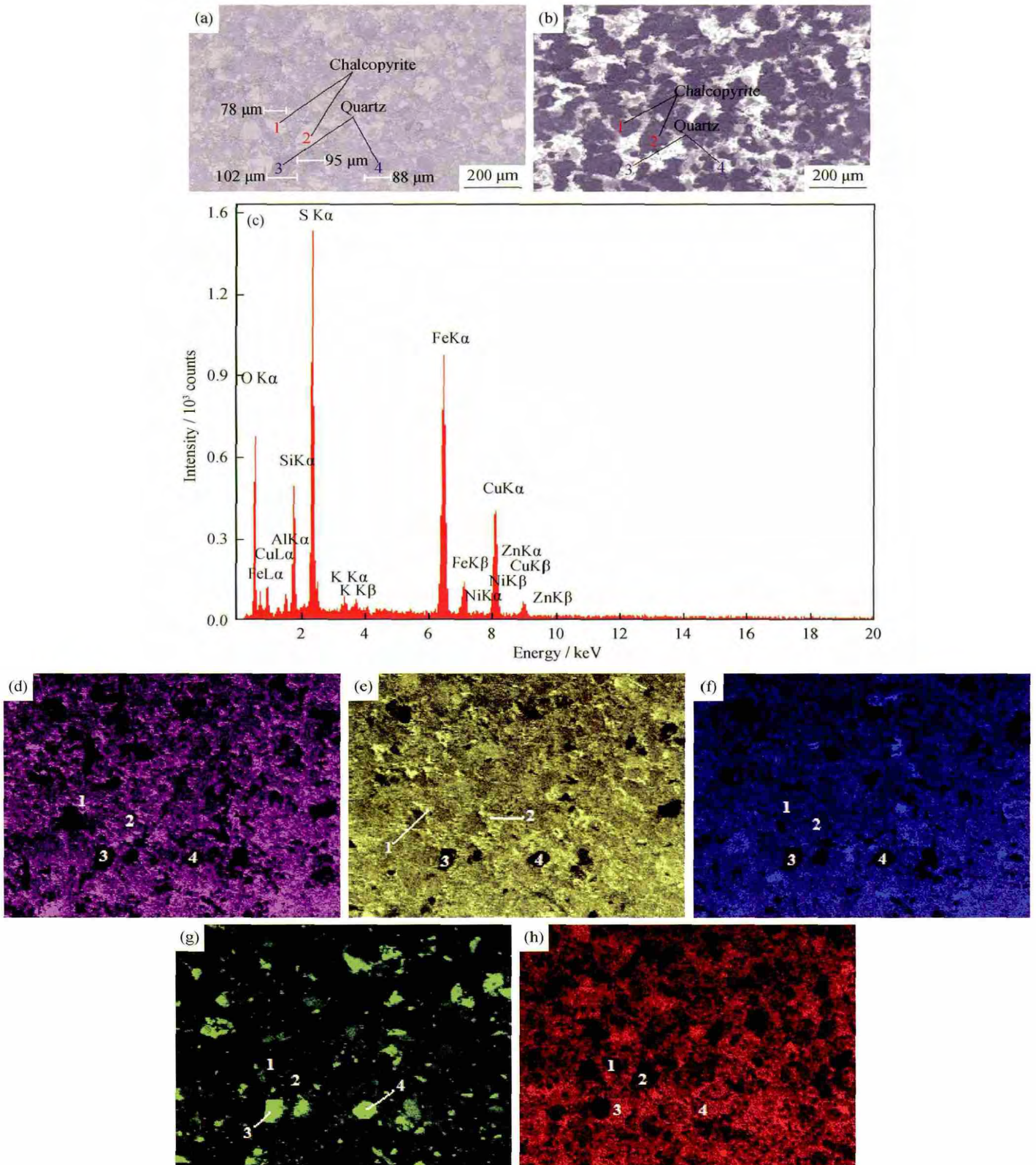

Fig. 2.   SEM images and EDX spectra of chalcopyrite concentrate: (a) SE image; (b) BSE image; (c) EDX spectrum; (d–h) elemental mapping for Cu, Fe, S, Si, and O, respectively.
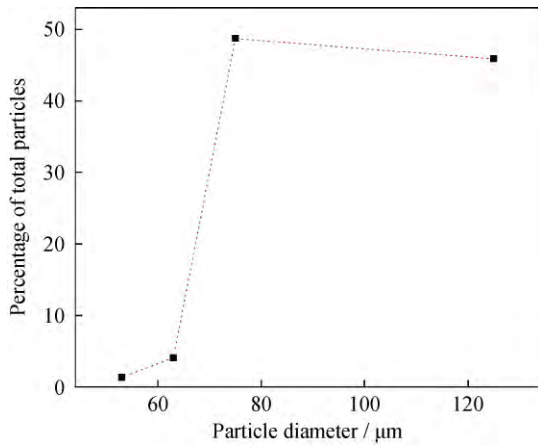
Fig. 3. Particle size distributions of chalcopyrite concentrate powder.

Table 2. Elemental analysis results of chalcopyrite concentrate by EDX   wt%

Cu	Fe	S	Si	O	Al	K	Ni	Zn
16.86	22.74	18.28	7.26	31.50	1.37	0.75	0.71	0.55

Table 3. FTIR data and band assignment

Observed IR frequency / cm^{-1}	Standard IR frequency / cm^{-1}	Band assignment
1621	1622 weak	SiO$_2$ hydrated amorphous silica
1204	1175 shoulder	Me–S absorb
1142	1135 shoulder	Me–S absorb
1105	1040–1090	Si–O–Si asymmetric stretch
	1110 weak	Me–S absorb
1010	1008	S–O stretch
886	885 very strong, 792 medium, 785–775 medium, 790–850	Si–O–Si symmetric stretch
798		
781		
630	628	S–O bend
625	628 strong shoulder, 600–650	Si–O–Si bend
580	570–68 weak	Si–O–Si absorb
411–515	440–465	Si–O–Si absorb

Note: weak (<20% absorption); shoulder (just resolved); very strong (>80% absorption); medium (<40% absorption); strong shoulder (approaching in intensity to the main absorption band).

3.4. Raman spectroscopic analysis

The Raman spectrum of the chalcopyrite concentrate is presented in Fig. 5, which was conducted in the low wavelength range (190–1550 cm^{-1}). The most prominent band occurs at 308 cm^{-1}, which can be characterized by the A$_1$ symmetry mode related to the tetrahedral clusters [CuS$_4$, FeS$_4$] of chalcopyrite. Two weaker bands appear at 320 and

353 cm^{-1}; these are related to the B$_2$ or E modes [15]. In contrast, the free (SO$_4$)$^{2-}$ ions have an ideal tetrahedral (T$_d$) symmetry. Two of the four fundamental vibrations coming from the group could be clearly observable at 1016 cm^{-1} (v_3) and 616 cm^{-1} (v_4). Also, the bands observed at 432 and 1335 cm^{-1} can be attributed to the presence of SO$_4$ [16]. The orthorhombic crystal structure of sulfur is a strong Raman scatterer, generating the bands in the region of 100–300 cm^{-1} due to S–S–S bending [15]. In the present case, these can be observed at 220, and 255 cm^{-1}. The high background noise in the region of 400–500 cm^{-1} is possibly due to the S–S stretching [17–18]. The band occurring at 631 cm^{-1} is due to an S–O bend.
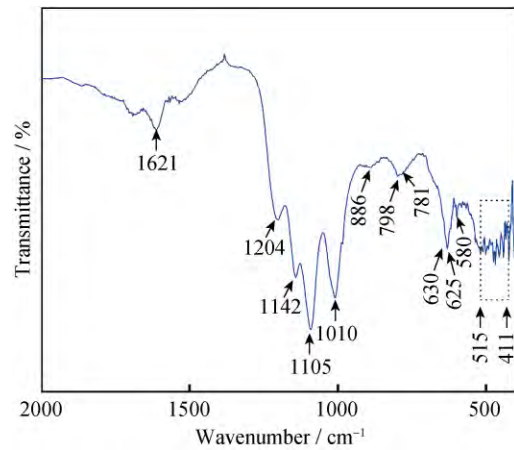

Fig. 4. FTIR spectrum of chalcopyrite concentrate recorded at room temperature.
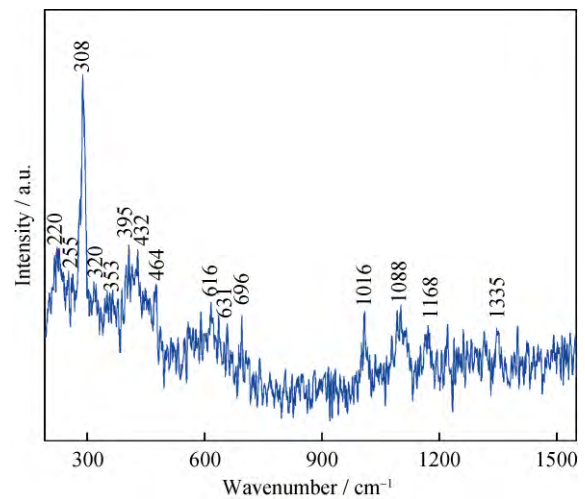

Fig. 5. Raman spectrum of chalcopyrite concentrate recorded at room temperature.

The main impurity phase in the sample as found in the diffraction and spectroscopic studies is silica (quartz). In good agreement, the band that occurs at 464 cm^{-1} in the Raman spectra is the characteristic band of quartz. Also, the

other bands occurring at 395, 696, 1088, and 1168 cm^{-1} establish the presence of silica in the concentrate sample [19–20].

3.5. UV-visible absorption spectral analysis

The optical absorption spectrum of the concentrate mineral powder dispersed in absolute alcohol, and measured in the 200–1100 nm wavelength range, is shown in Fig. 6. The absorption band at 360 nm, corresponding to a band gap of 3.4 eV, appears for CuFeS$_2$; this can be assigned to Cu(II) in the rhombic symmetry. Another band is observed at 310 nm (4 eV), which is an energy characteristic of Fe^{3+} transition. The experimental values are comparable with the values reported in the literatures [21–23].
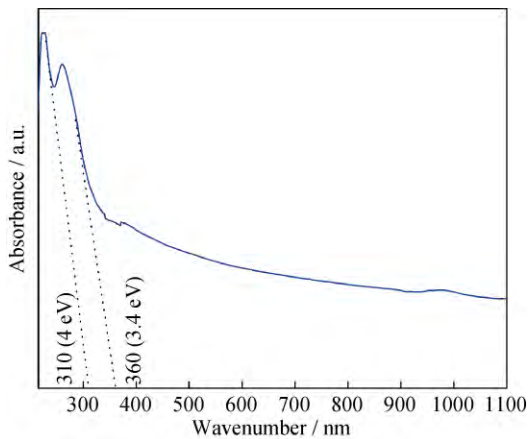

Fig. 6.   Optical absorption spectra of chalcopyrite concentrate recorded at room temperature.

3.6. Thermal analysis

DTA and TG plots obtained during heating of the chalcopyrite concentrate powder from room temperature (303 K) to 1273 K are shown in Fig. 7. At about 368 K, the onset of an endothermic peak occurs in the DTA curve, suggesting the elimination of hydrated water from the concentrate. A weight loss of less than 5% in TG corresponds to this phenomenon. The onset of the next thermal event happens at 658 K, which is due to the decomposition of chalcopyrite. This process is endothermic [24], and corresponds to about 20% weight loss in TG, which is mainly due to the removal of sulfur from the chalcopyrite. The next two endothermic peaks occur at the onset temperatures of 848 K and 1145 K, which appear due to the structural change of SiO$_2$. The first one corresponds to the transformation of low quartz (α-SiO$_2$) to high quartz (β-SiO$_2$), and the second one corresponds to the transformation of β-SiO$_2$ to cristobalite (γ-SiO$_2$) [25]. The low quartz phase appeared in the powder XRD pattern at the room temperature, as discussed earlier.
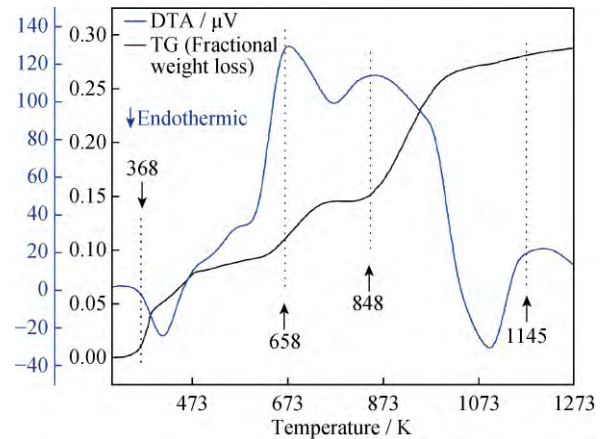

Fig. 7.   TG-DTA plot of chalcopyrite concentrate heated from room temperature to 1273 K.

Fig. 8 shows a TG–DTG plot of the concentrate powder in the temperature region of the decomposition of chalcopyrite. H_m, T_m, and x_m denote the peak height, peak temperature, and weight conversion at peak temperature, respectively (subscript m stands for maxima). The first two are obtained from the DTG curve, and the last one from the corresponding TG plot. The values are found to be $H_m =$ 0.05181 K^{-1}, $T_m =$ 657.44 K, which is in good agreement with the DTA result, and $x_m =$ 0.10595. The activation energy (E_a) is calculated using the relation $E_a = RT_m^2 H_m /$ $(1 - x_m)$, which is valid for the first order chemical reaction [26], R being the universal gas constant. The value is 208 kJ·mol^{-1}. The value is close to the one reported in the literature [22], which may be expected since x_m rarely varies with the heating rate [27].
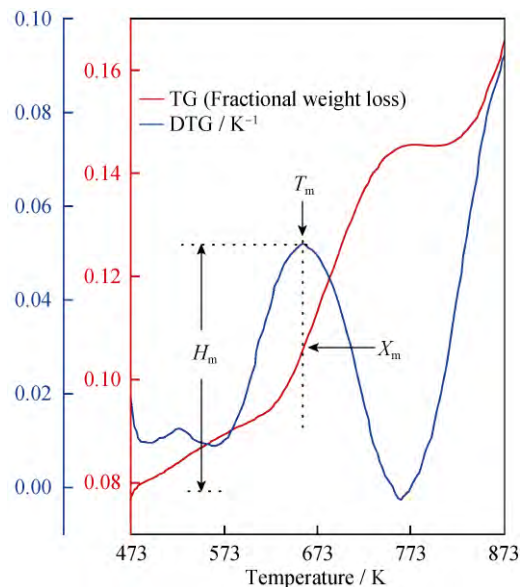

Fig. 8.   TG-DTG plot of chalcopyrite concentrate from 473 K to 873 K.

4. Conclusion

Powder XRD pattern of a Ghatsila chalcopyrite concentrate indicates that the main phase present in it is free chalcopyrite, with low quartz as the major impurity. This is confirmed by Rietveld refinement of the XRD data. The refined lattice parameters are $a = 0.5290181$ nm, $b = 0.5290181$ nm, and $c = 1.042317$ nm for $CuFeS_2$; and $a = 0.4920487$ nm, $b = 0.4920487$ nm, and $c = 0.5391766$ nm for $\alpha\text{-}SiO_2$. The weight ratio of the two phases is found to be approximately 3:1, which is in good agreement with the prediction of the EDX analysis of the concentrate. The particle size of the concentrate powder is about 100 µm, according to both the SEM images and sieve analysis. Spectroscopic studies show the presence of tetrahedral clusters [CuS_4, FeS_4] in the mineral, and a small presence of the S–O absorption, which indicates oxidation of a small fraction of sulfide. Also, the characteristic absorption bands of quartz at the 1040–1090 cm^{-1} range are observed in the concentrate spectra. The band gap of the concentrate is found to be 3.4 eV. The thermal analysis shows three successive thermal events: (1) removal of moisture near 368 K; (2) decomposition of $CuFeS_2$ at 658 K. The activation energy associated with the endothermic phenomena calculated from the DTG curve is 208 kJ·mol^{-1}; and (3) changes of the crystal structure of SiO_2, namely the formation of high quartz from the room temperature phase (low quartz) at 848 K, and the formation of cristobalite from high quartz at 1145 K.

Acknowledgements

References

[1] W.D. Nesse, *Introduction to Mineralogy*, Oxford University Press, Oxford, 2000, p. 1.

[2] A.A. Baba, K.I. Ayinla, F.A. Adekola, R.B. Bale, M.K. Ghosh, A.G.F. Alabi, A.R. Sheik, and I.O. Folorunso, Hydrometallurgical application for treating a Nigerian chalcopyrite ore in chloride medium: Part I. Dissolution kinetics assessment, *Int. J. Miner. Metall. Mater.*, 20(2013), No. 11, p. 1021.

[3] R. Chatterjee and D. Ghosh, Characterization of Cu–SiO$_2$ composite synthesized by hydrogen reduction of chalcopyrite concentrate followed by acid leaching, *Metall. Mater. Trans. B*, 44(2013), No. 5, p. 1049.

[4] A.A. Baba, K.I. Ayinla, F.A. Adekola, M.K. Ghosh, O.S. Ayanda, R.B. Bale, A.R. Sheik, and S.R. Pradhan, A review on novel techniques for chalcopyrite ore processing, *Int. J. Min. Eng. Miner. Process.*, 1(2012), No. 1, p. 1.

[5] A. Le Bail, H. Duroy, and J.L. Fourquet, *Ab-initio* structure determination of LiSbWO$_6$ by X-ray powder diffraction, *Mater. Res. Bull.*, 23(1988), No. 3, p. 447.

[6] V. Petricek, M. Dusek, and L. Palatinus, JANA2006 *The Crystallographic Computing System*, Institute of Physics, Praha, Czech Republic, 2011.

[7] P. Baláž, *Mechanochemistry in Nanoscience and Minerals Engineering*, Springer Berlin Heidelberg, 2008, p. 136.

[8] K. Omori, *Science Reports*, 3rd Ser., Vol.9, No.1, Tohoku University, 1964, p. 65.

[9] K. Omori, *Science Reports*, Vol.7, Tohoku University, 1961, p.101.

[10] J. Leppinen, FTIR and flotation investigation of the adsorption of ethyl xanthate on activated and non-activated sulfide minerals, *Int. J. Miner. Process.*, 30(1990), No. 3-4, p. 245.

[11] D.H. Sepehrian, A.R. Khanchi, M.K. Rofouei, and S.W. Husain, Non-thermal synthesis of mesoporous zirconium silicate and its characterization, *J. Iran. Chem. Soc.*, 3(2006), p. 253.

[12] J.A. Gadsen, *Infrared Spectra of Minerals and Related Inorganic Compounds*, Butterworths, London, 1975, p. 46.

[13] T. Ishizaki, N. Saito, Y. Inoue, M. Bekke, and O. Takai, Fabrication and characterization of ultra-water-repellent alumina-silica composite films, *J. Phys. D.*, 40(2007), p. 192.

[14] A. Beran, G. Giester, and E. Libowitzky, The hydrogen bond system in natrochalcite-type compounds: an FTIR spectroscopic study of the H$_3$O$_2$ unit, *Mineral. Petrol.*, 61(1997), No. 1-4, p. 223.

[15] X. Fontané, L. Calvo-Barrio, V. Izquierdo-Roca, E. Saucedo, A. Pérez-Rodriguez, J.R. Morante, D.M. Berg, P.J. Dale, and S. Siebentritt, In-depth resolved Raman scattering analysis for the identification of secondary phases: characterization of Cu$_2$ZnSnS$_4$ layers for solar cell applications, *Appl. Phys. Lett.*, 98(2011), No. 18, art. No. 181905.

[16] G. Udayabhaskar Reddy, K. Seshamaheswaramma, Y. Nakamura, S. Lakshmi Reddy, R.L. Frost, and T. Endo, Electron paramagnetic resonance, optical absorption and Raman spectral studies on a pyrite/chalcopyrite mineral, *Spectrochim. Acta Part A*, 96(2012), p. 310.

[17] G.A. Ozin, The single-crystal Raman spectrum of rhombic sulphur, *J. Chem. Soc. A*, (1969), p. 116.

[18] P.D. Harvey and I.S. Butler, Raman spectra of orthorhombic sulfur at 40 K, *J. Raman Spectrosc.*, 17(1986), No. 4, p. 329.

[19] P. Gillet, A. Le Cléac'h, and M. Madon, High-temperature Raman spectroscopy of SiO$_2$ and GeO$_2$ polymorphs: anharmonicity and thermodynamic properties at high-temperatures, *J. Geophys. Res.*, 95(1990), No. B13, p. 21635.

[20] R.J. Hemley, Pressure dependence of Raman spectra of SiO$_2$ polymorphs: alpha-quartz, coesite and stishovite, [in]

High-Pressure Research in Mineral Physics: *a Volume in Honor of Syun-iti Akimoto*, American Geophysical Union, 2013, p.347.

[21] S.D. Disale and S.S. Garje, A convenient synthesis of nanocrystalline chalcopyrite, $CuFeS_2$ using single-source precursors, *Appl. Organomet. Chem.*, 23(2009), No. 12, p. 492.

[22] B. Prameena, G. Anbalagan, S. Gunasekaran, G.R. Ramkumaar, and B. Gowtham, Structural, optical, electron paramagnetic, thermal and dielectric characterization of chalcopyrite, *Spectrochim. Acta Part A*, 122(2014), p. 348.

[23] D.M. Sherman and T.D. Waite, Electronic spectra of Fe^{3+} oxides and oxide hydroxides in the near IR to near UV, *Am.*

Mineral., 70(1985), No. 11-12, p. 1262.

[24] A. Roine, *Outokumpu HSC Chemistry for Windows*: *Chemical Reaction and Equilibrium Software with Extensive Thermochemical Database*, Pori, Finland, 1999.

[25] H. Okamoto, O–Si (oxygen–silicon), *J. Phase Equilib.Diffus.*, 28(2007), p. 309.

[26] S. Kim and J.K. Park, Characterization of thermal reaction by peak temperature and height of DTG curves, *Thermochim. Acta*, 264(1995), p. 137.

[27] J.H. Flynn and L.A. Wall, General treatment of the thermogravimetry of polymers, *J. Res. Natl. Bur. Stand.*, 70A(1966), No. 6, p. 487.